# Algorithms for surface reconstruction from curvature data for freeform aspherics

Dae Wook Kim*[a], ByoungChang Kim[b], Chunyu Zhao[a], ChangJin Oh[a] and James H. Burge[a]

[a] College of Optical Sciences, University of Arizona, Tucson, Arizona 85721, USA
[b] School of Mechanical Engineering, Kyungnam University, Changwon 631-701, South Korea

## ABSTRACT

Increasing demand for highly accurate freeform aspheric surfaces requires accurate and efficient measurement techniques. One promising possibility uses a sub-aperture scanning system that measures local curvature variations across the part. In this paper, we develop and demonstrate two different data processing algorithms, a zonal approach using Southwell integration method and a modal approach leveraging Zernike curvature basis, that reconstruct the surface 3-dimensional profiles from the curvature data. The performance of suggested methods and the sensitivity to noise is diagnosed for various SNR (Signal-to-Noise Ratio) cases.

**Keywords:** Aspheric metrology, curvature sensing, optical testing, freeform aspherics

## 1. INTRODUCTION

Optical components that use freeform surfaces require special techniques for metrology. Surfaces are required to be measured accurately, yet they may have no symmetry and may have large departure from spherical. Coordinate measuring machines can measure such surfaces, but with limited spatial sampling and accuracy.[1] Full aperture interferometry with CGH (Computer Generated Hologram) provides highly accurate measurements, but requires a custom CGH for each part.[2] Sub-aperture interferometry coupled with stitching software can provide surface reconstruction for some classes of surfaces.[3]

We introduce and discuss data reduction for a different class of sub-aperture interferometer that samples very small regions of the surface to determine the local curvature. Such instruments and algorithms that provide curvature along one direction and integrate this to determine optical surface shape profiles have been highly successful.[4-6] We reference the GEMM[6] (Geometry Measuring Machine) in figure 1 developed at NIST (National Institute of Standards and Technology) that uses interferometry to sample all three second derivatives across full freeform optical surfaces.

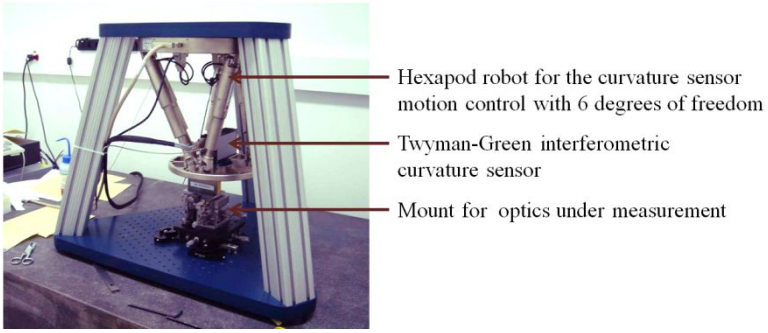


Figure 1. GEMM (Geometry Measuring Machine) developed at NIST (National Institute of Standards and Technology), which measures local curvature along a scanning line to reconstruct the freeform optical surface profile [6]

* letter2dwk@hotmail.com

Optical Manufacturing and Testing X, edited by Oliver W. Fähnle, Ray Williamson,
Dae Wook Kim, Proc. of SPIE Vol. 8838, 88380B · © 2013 SPIE
CCC code: 0277-786X/13/$18 · doi: 10.1117/12.2024285

A circular sub-aperture surface shape $f_{sub}(x, y)$ about its center $(0, 0)$ can be expressed using Taylor series expansion as

$$f_{sub}(x,y) = f_{sub}(0,0) + x\frac{\partial f_{sub}(0,0)}{\partial x} + y\frac{\partial f_{sub}(0,0)}{\partial y} + \frac{1}{2!}[x^2\frac{\partial^2 f_{sub}(0,0)}{\partial x^2} + 2xy\frac{\partial^2 f_{sub}(0,0)}{\partial x \partial y} + y^2\frac{\partial^2 f_{sub}(0,0)}{\partial y^2}] + \ldots \quad (1)$$

At the same time, $f_{sub}(x, y)$ can be represented in terms of Zernike polynomials, which is a complete and orthogonal basis over a normalized unit circle, as

$$f_{sub}(x,y) = \sum_n a_n \cdot Z_n(x,y), \quad (2)$$

where $a_n$ is the $n$-th Zernike coefficient and $Z_n$ is the $n$-th Zernike basis function defined as

$$\begin{aligned} Z_1 &= 1 && \text{(Piston)} \\ Z_2 &= x, \quad Z_3 = y && \text{(Tip and tilt)} \\ Z_4 &= 2x^2 + 2y^2 - 1 && \text{(Power)} \\ Z_5 &= 2xy, \quad Z_6 = x^2 - y^2 && \text{(Astigmatism)} \\ &\ldots \end{aligned} \quad (3)$$

The first 6 Zernike polynomials are shown in figure 2.

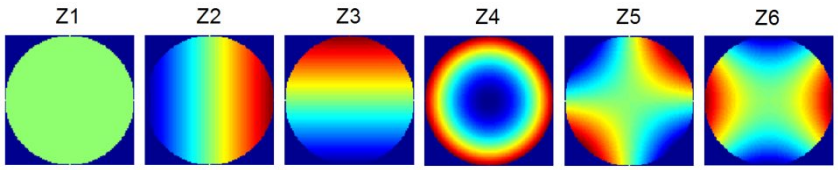


Figure 2. The first 6 Zernike polynomials within a unit (radius = 1) circle area (Blue to Red: -1 to 1)

By comparing equation (1) and (2) term by term, the three second derivative values ($d_{xx}$, $d_{xy}$ and $d_{yy}$) in the local sub-aperture region can be determined in terms of power and two astigmatism Zernike coefficients, $a_4$, $a_5$ and $a_6$ as

$$d_{xx} \equiv \frac{\partial^2 f_{sub}(0,0)}{\partial x^2} = 4a_4 + 2a_6 \;,\; d_{xy} \equiv \frac{\partial^2 f_{sub}(0,0)}{\partial x \partial y} = 2a_5 \;\; and \;\; d_{yy} \equiv \frac{\partial^2 f_{sub}(0,0)}{\partial y^2} = 4a_4 - 2a_6 . \quad (4)$$

In this paper, we discuss the form of the second derivative data (i.e. curvature vector) and provide two different methods of processing curvature data to reconstruct the surface maps. A two-step integration algorithm using Southwell's zonal approach[7] is provided that maintains high spatial resolution of the data. Another technique utilizing Zernike curvature basis[8] is provided that offers a convenient modal reconstruction approach to fit the curvature data. The performance of these algorithms is evaluated and compared.

## 2. REPRESENTATION OF CURVATURE DATA

A synthetic 0.2m diameter freeform surface with ~0.8mm maximum sag difference was generated as shown in figure 3 (top-left) and used for various simulations in this paper. Three ideal second derivative maps of the synthetic surface were also calculated and presented in figure 3. The $d_{xx}$ and $d_{yy}$ represent the second derivatives of the surface map in x and y direction while $d_{xy}$ contains the cross-term information of the curvature. The sampling was made on 501 by 501 grid points equally spaced over the synthetic surface. The three second derivative values at those local sampling points across the freeform surface produce a curvature vector $\vec{c}(x, y)$ defined as $[d_{xx}(x, y), d_{xy}(x, y), d_{yy}(x, y)]$, where $(x, y)$ is the coordinates of the sampling locations.

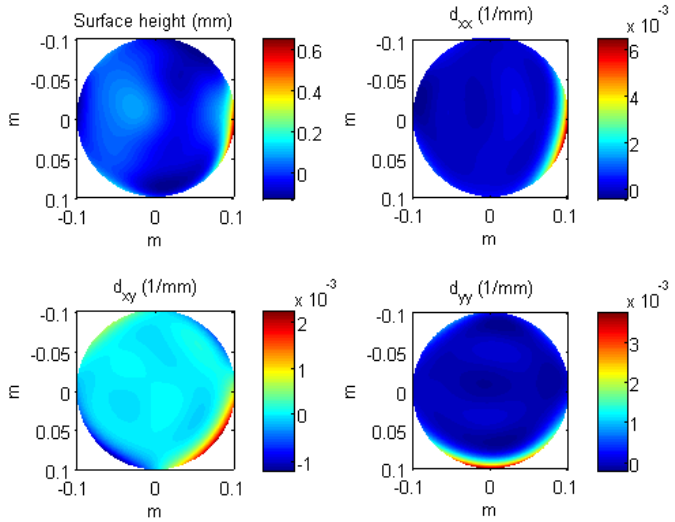


Figure 3. Synthetic 0.2m diameter freeform aspheric surface (top-left) and its ideal curvature vector $\vec{c}$ components $[d_{xx}(x, y), d_{xy}(x, y), d_{yy}(x, y)]$ containing the local second derivative values on the 501 by 501 sampling grid

The curvature vector $\vec{c}(x, y)$, in practice, could be measured using various curvature sensors mounted on a scanning system. The measured $\vec{c}(x, y)$ is used to reconstruct the original surface map $f(x, y)$ utilizing different data reduction approaches discussed in Section 3.

## 3. SURFACE RECONSTRUCTION

### 3.1 Zonal Approach: Two-step Integration using Southwell Method

A synthetic freeform surface reconstruction using a zonal approach was simulated. Two-step integration was applied using Southwell method[7]. The first two curvature vector components $d_{xx}$ and $d_{xy}$ were integrated to get the x-slope map of the original surface. In the same way, y-slope map was calculated by integrating $d_{xy}$ and $d_{yy}$. Those two slope maps went through the second Southwell integration step to reconstruct the original surface shape. A schematic diagram showing the flow of this two-step zonal approach is presented in figure 4.

Starting from the ideal (i.e. noise-free) curvature vector in figure 3, the 0.2m synthetic surface map was successfully reconstructed. A comparison between the original synthetic surface and the reconstructed result is presented in figure 5 with the reconstruction error (i.e. difference between the original and the reconstructed surface). As the input data was noise-free, the reconstruction error map represents the intrinsic error associated with the numerical zonal integration method used in this study.

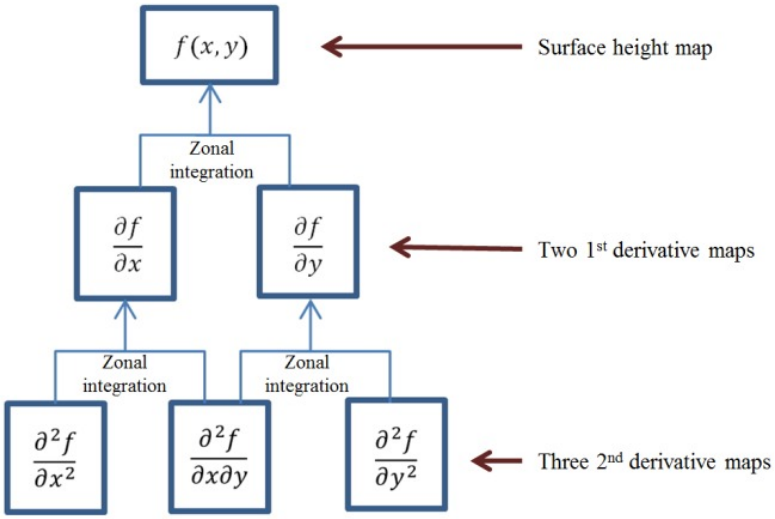


Figure 4. Schematic block diagram showing the two-step zonal integration process using Southwell method

The piston and tip-tilt terms have been subtracted from the maps as the curvature-based reconstruction is fundamentally blind to those terms. In other words, the second derivatives do not maintain any information about the surface's piston and tip-tilt components. The reconstructed surface's RMS (Root-Mean-Square) 0.080461mm is almost same as the original surface RMS 0.080449mm. The reconstruction error map shows only ~0.000019mm RMS residual difference as shown in figure 5 (right).

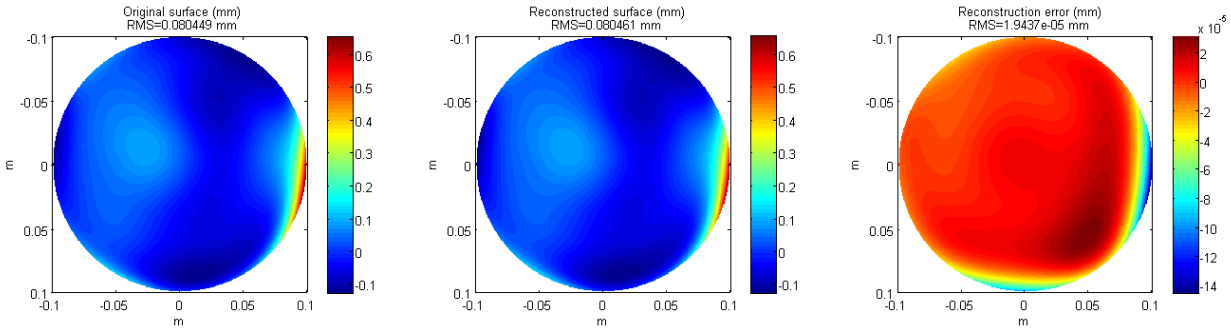


Figure 5. Zonal reconstruction result using Southwell method: Original synthetic surface (left), reconstructed surface (middle) and reconstruction error map (right) *(Note: The piston and tip-tilt have been subtracted from the maps. The reconstruction error is the difference between the original and the reconstructed surface.)*

### 3.2 Modal Approach: Fitting using Zernike Curvature Basis

A new Zernike curvature basis[8], *C* polynomial, has been defined and used to demonstrate the modal approach for a surface reconstruction. This method directly fits the curvature vector using the orthogonal basis and produces the analytical description of the original surface. The overall data processing flow is summarized in figure 6.

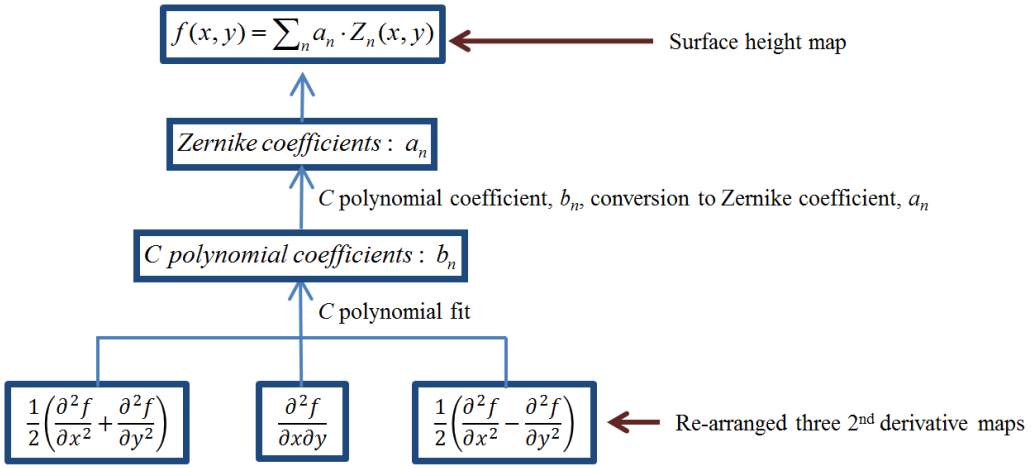


Figure 6. Schematic block diagram showing the modal reconstruction approach using Zernike curvature basis

The three second derivative components in the curvature vector $\vec{c}(x, y)$ are slightly re-arranged to form a vector

$$\vec{c}'(x,y)=\begin{pmatrix}\frac{1}{2}\left(\frac{\partial^2 f}{\partial x^2}+\frac{\partial^2 f}{\partial y^2}\right)\\ \frac{\partial^2 f}{\partial x \partial y}\\ \frac{1}{2}\left(\frac{\partial^2 f}{\partial x^2}-\frac{\partial^2 f}{\partial y^2}\right)\end{pmatrix}, \tag{5}$$

which can be fitted to the curvature *C* polynomials (orthonormal over a circular domain) as

$$\vec{c}'(x,y)=\sum_n b_n \cdot \vec{C}_n(x,y), \tag{6}$$

where $b_n$ is the *n*-th *C* polynomial coefficient and $\overrightarrow{C_n}$ is the *n*-th *C* polynomial basis function.[8] Since each term in *C* polynomials is a combination of the second derivatives of Zernike polynomials, the scalar function *f(x, y)* that represents the surface whose second derivatives are $\vec{c}'(x,y)$ can be written in terms of Zernike polynomials as

$$f(x,y)=\sum_n a_n \cdot Z_n(x,y), \tag{7}$$

where coefficients $a_n$ are directly calculated from coefficients $b_n$.

For a comparison with the zonal approach in Section 3.1, the identical synthetic map was reconstructed via the modal fit approach using same ideal curvature vector. The reconstructed surface (middle) and the reconstruction error (right) is presented in figure 7. Similar to the zonal case in figure 5, the reconstruction error for this noise-free case is very small (practically 0) as shown in the figure 7 reconstruction error (right). This error value provides a good baseline to evaluate other cases simulating certain noise levels for the curvature data in Section 4.

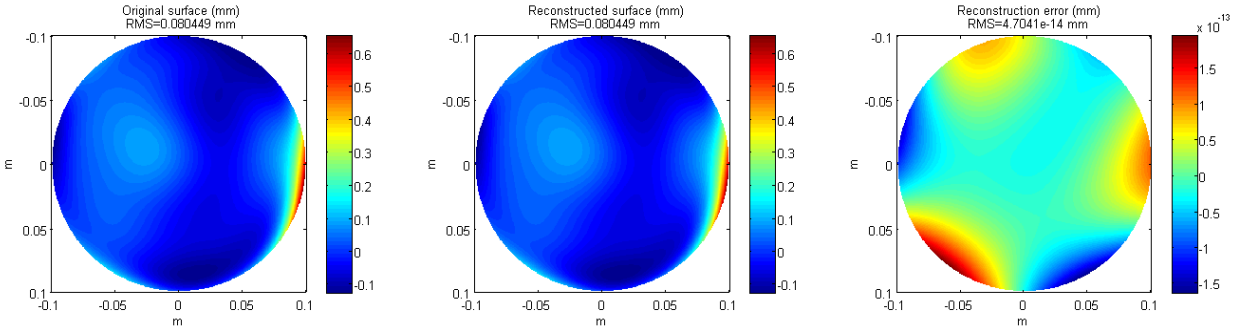


Figure 7. Modal reconstruction result using Zernike curvature basis: Original synthetic surface (left), reconstructed surface (middle) and reconstruction error map (right) *(Note: The piston and tip-tilt have been subtracted from the maps. The reconstruction error is the difference between the original and the reconstructed surface.)*

# 4. PERFORMANCE ANALAYSIS OF DATA REDUCTION TECHNIQUES

## 4.1 Noise Rejection during Reconstruction Process

A noise rejection analysis for the two reconstruction approaches (zonal and modal method) in Section 3 has been conducted using simulated noisy curvature data. In practice, curvature data noise may come from various sources including curvature sensor noise, finite size sub-aperture area and numerical fitting errors during a local curvature determination.

Three different levels of SNR (Signal-to-Noise Ratio) cases were examined. Gaussian random noise statistics were assumed for the curvature noise from a sampling location to another location. The SNR was defined as ratio of mean magnitude curvature to standard deviation $\sigma$ of the Gaussian random noise. Three different curvature vectors for SNR=1, 4, and 16 cases were generated and the three components for SNR=1 curvature vector case are presented in figure 8 as an example.

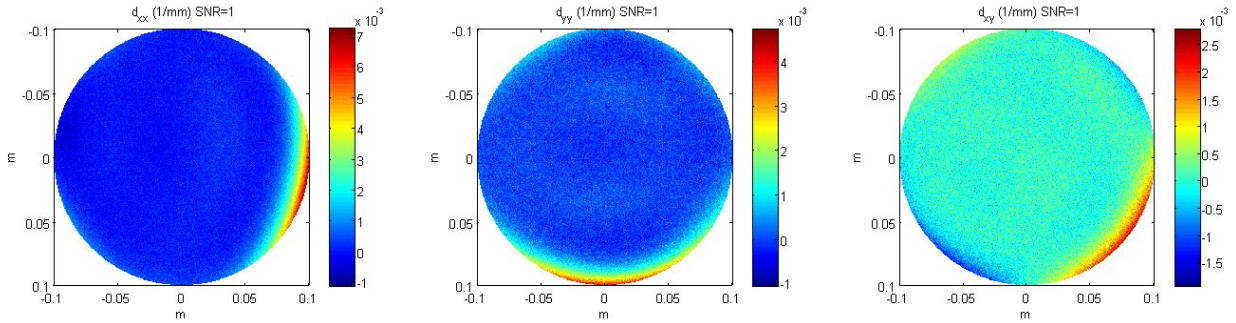


Figure 8. Three curvature vector components, $d_{xx}$, $d_{yy}$, and $d_{xy}$ for Gaussian random noise of SNR=1 case

Each curvature vector was fed in to both the Southwell integration routine and the Zernike curvature basis modal fit routine, separately. Both simulation results showing the reconstructed surface with their residual reconstruction error for SNR=1 case are compared in figure 9 (top vs. bottom). For both approaches, in general, the reconstructed surfaces were very similar to the true answer (i.e. original surface) even if the added curvature noise level was comparable to the true signal magnitude (i.e. SNR=1). It is important to note that this result depends on the number of sampling points. (Additional study result using different sampling rate is presented in Section 4.2.) The propagated noise effects in the reconstructed surface are well observed in the reconstruction error maps.

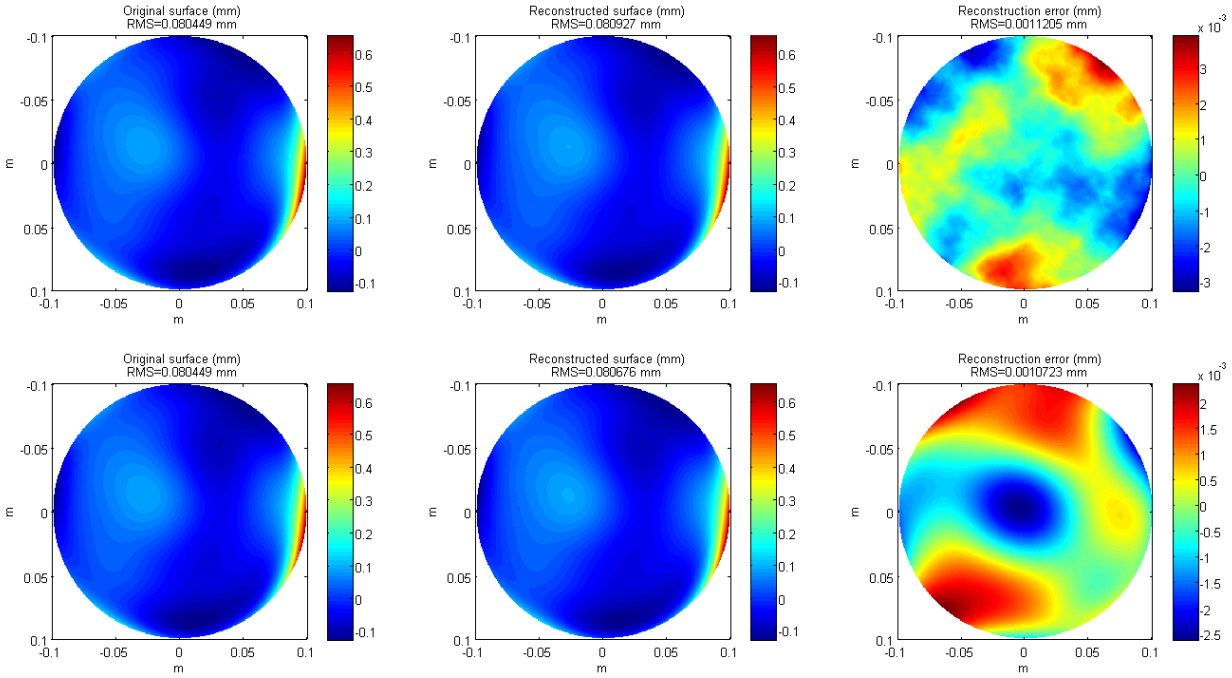


Figure 9. Reconstruction performance comparison in terms of noise rejection (SNR=1 case): Southwell integration result (top row) and Zernike curvature basis modal fit result (bottom row). Original synthetic surface (left), reconstructed surface (middle) and reconstruction error (right). *(Note: piston and tip-tilt have been subtracted from the maps.)*

The results for all SNR cases are summarized in table 1. A performance criterion, normalized reconstruction error $\varepsilon$, was defined as

$$\varepsilon \equiv \frac{RMS_{reconstruction\_error}}{RMS_{original\_surface}} \cdot 100 \ [\%] \ . \tag{8}$$

It was demonstrated that both approaches give very good <0.25% normalized reconstruction error for the high SNR=16 case. As the SNR becomes low (SNR=1), $\varepsilon$ goes up to ~1.4%. Both the Southwell-based zonal approach and the *C* polynomial-based modal approach demonstrated their high noise rejection capability in these simulations.

Table 1. Normalized reconstruction error $\varepsilon$ comparison between the zonal and modal approach (501 by 501 sampling)

| **SNR** | **Original surface RMS (mm)** | **Zonal approach** | | **Modal approach** | |
|---|---|---|---|---|---|
| | | Reconstruction error RMS (mm) | Normalized reconstruction error $\varepsilon$ [a] (%) | Reconstruction error RMS (mm) | Normalized reconstruction error $\varepsilon$ [a] (%) |
| 1 | 0.080449 | 0.001120 | 1.39 | 0.001072 | 1.33 |
| 4 | 0.080449 | 0.000392 | 0.49 | 0.000558 | 0.69 |
| 16 | 0.080449 | 0.000197 | 0.24 | 0.000175 | 0.22 |
| $\infty$ [b] | 0.080449 | 0.000019 | 0.02 | 0.000000 | 0.00 |

[a] Normalized reconstruction error $\varepsilon$ defined in equation (8).

[b] This case represents the intrinsic errors belongs to the reconstruction method shown in figure 5 and 7.

### 4.2 Spatial Sampling Frequency Analysis

The spatial sampling frequency of the curvature vector is another critical factor affecting the reconstruction performance in the presence of noise. It not only defines the spatial resolution of the reconstructed surface map (for the zonal approach), but also affects the robustness of the reconstruction process against noisy curvature data discussed in Section 4.1. Identical sets of simulations using same data with half sampling rate in each direction (251 by 251 sampling grid over the curvature vector component map) were performed. In other words, the size of each curvature vector component, $d_{xx}$, $d_{xy}$ and $d_{yy}$, became 1/4. The simulation results are summarized and presented in table 2.

Table 2. Normalized reconstruction error $\varepsilon$ comparison between the zonal and modal approach (251 by 251 sampling)

| SNR | Original surface RMS (mm) | Zonal approach | | Modal approach | |
|---|---|---|---|---|---|
| | | Reconstruction error RMS (mm) | Normalized reconstruction error $\varepsilon$ [a] (%) | Reconstruction error RMS (mm) | Normalized reconstruction error $\varepsilon$ [a] (%) |
| 1 | 0.076452 | 0.002833 | 3.70 | 0.004448 | 5.80 |
| 4 | 0.076452 | 0.000859 | 1.12 | 0.000914 | 1.20 |
| 16 | 0.076452 | 0.000251 | 0.32 | 0.000287 | 0.38 |
| ∞ | 0.076452 | 0.000072 | 0.09 | 0.000000 | 0.00 |

[a] Normalized reconstruction error $\varepsilon$ defined in equation (8).

In comparison to the original sampling rate case in table 1, it is obvious that the overall normalized reconstruction error got worse by factor of ~2.6-2.7 for both the zonal and modal approaches. Also, the modal approach showed slightly higher $\varepsilon$ values compared to the zonal case. However, we acknowledge that more rigorous statistical analysis (not just 8 case studies) such as Monte Carlo simulation is required to draw more general conclusion about these noise rejection characteristics. Detailed analysis and further discussions are planned to be provided in a separate paper. [9]

## 5. CONCLUSION

Surface measurements that sample curvature do not rely one precise mechanical positioning, therefore they can be made nearly insensitive to alignment and vibration. A number of successful scanning systems have been developed to utilize this advantage. The integration of profile curvature data is straightforward. We evaluate two classes of algorithms that integrate full curvature data sampled over the full aperture. Direct integration using two iterations of Southwell's method proves to be robust, and maintains the full resolution of the data. A modal technique was also explored, where curvature basis functions are fit to the data. These functions have one-to-one correspondence with surface functions, allowing a direct computation from the curvature coefficients. The initial evaluation shown here demonstrates both techniques to have surprisingly good noise rejection. This work will be followed up by analysis that provides parametric relationships for the performance.

## REFERENCES


[1] P. Su, C. J. Oh, R. E. Parks, and J. H. Burge, "Swing arm optical CMM for aspherics," Proc. SPIE **7426** (2009).

[2] J. H. Burge, "Applications of computer-generated holograms for interferometric measurement of large aspheric optics," Proc. SPIE **2576** (1995).

[3] P. Murphy, J. Fleig, G. Forbes, D. Miladinovic, G. DeVries, and S. O'Donohue, "Subaperture stitching interferometry for testing mild aspheres", Proc. SPIE **6293** (2006).

[4] P. E. Glenn, "Angstrom level profilometry for submillimeter- to meter-scale surface errors," Proc. SPIE **1333** (1990).

[5] W. Zou, K. P. Thompson, and J. P. Rolland. "Differential Shack-Hartmann curvature sensor: local principal curvature measurements," JOSA A **25** (9), 2331-2337 (2008).

[6] U. Griesmann, N. Machkour-Deshayes, J. Soons, B. C. Kim, Q. Wang, J. R. Stoup, and L. Assoufid, "Uncertainties in aspheric profile measurements with the geometry measuring machine at NIST," Proc. SPIE **5878** (2005).
[7] W. H. Southwell, "Wavefront estimation from wave-front slope measurements," JOSA **70** (8), 998–1006 (1980).
[8] C. Zhao and J. H. Burge, "Orthonormal curvature polynomials in a unit circle: basis set derived from curvatures of Zernike polynomials," submitted to Optics Express.
[9] D. W. Kim, C. Zhao and J. H. Burge are preparing a manuscript to be called "Curvature-based freeform surface metrology."